^{136}Ba studied via deep-inelastic collisions: Identification of the $(\nu h_{11/2})^{-2}_{10^+}$ isomer

J. J. Valiente-Dobón,[1,*] P. H. Regan,[1,2] C. Wheldon,[1,3] C. Y. Wu,[4] N. Yoshinaga,[5] K. Higashiyama,[5] J. F. Smith,[6] D. Cline,[4] R. S. Chakrawarthy,[6] R. Chapman,[7] M. Cromaz,[8] P. Fallon,[8] S. J. Freeman,[6] A. Görgen,[8] W. Gelletly,[1] A. Hayes,[4] H. Hua,[4] S. D. Langdown,[1,2] I. Y. Lee,[8] X. Liang,[7] A. O. Macchiavelli,[8] C. J. Pearson,[1] Zs. Podolyák,[1] G. Sletten,[9] R. Teng,[4] D. Ward,[8] D. D. Warner,[10] and A. D. Yamamoto[1,2]

[1]*Department of Physics, University of Surrey, Guildford GU2 7XH, United Kingdom*

[2]*Wright Nuclear Structure Laboratory, Yale University, New Haven, Connecticut 06520-8124, USA*

[3]*Kernphysik II, GSI, Max-Plank-Straße 1, D-64291 Darmstadt, Germany*

[4]*Department of Physics, University of Rochester, New York 14627, USA*

[5]*Department of Physics, Saitama University, Saitama City 338-8570, Japan*

[6]*Department of Physics and Astronomy, Schuster Laboratory, University of Manchester, Manchester M13 9PL, United Kingdom*

[7]*Department of Electronic Engineering and Physics, University of Paisley, Paisley PA1 2BE, United Kingdom*

[8]*Lawrence Berkeley National Laboratory, Berkeley, California 94720, USA*

[9]*The Niels Bohr Institute, University of Copenhagen, Blegdamsvej 17, 2100 Copenhagen, Denmark*

[10]*CCLRC Daresbury Laboratory, Warringdon WA 4AD, United Kingdom*

(Received 26 September 2003; published 27 February 2004)

A multinucleon transfer reaction between a thin self-supporting $^{198}_{78}$Pt target and an 850 MeV $^{136}_{54}$Xe beam has been used to populate and study the structure of the $N=80$ isotone $^{136}_{56}$Ba. Making use of time-correlated γ-ray spectroscopy, evidence for an $I^{\pi}=(10^+)$ isomeric state has been found with a measured half-life of 91 ± 2 ns. Prompt-delayed correlations have also enabled the tentative measurement of the near-yrast states which lie above the isomer. Shell-model calculations suggest that the isomer has a structure which can be assigned predominantly as $(\nu h_{11/2})^{-2}_{10^+}$. The results are discussed in terms of standard and pair-truncated shell-model calculations, and compared to the even-Z $N=80$ isotones ranging from $^{130}_{50}$Sn to $^{148}_{68}$Er. A qualitative explanation of the observed dramatic decrease in the $B(E2:10^+\rightarrow 8^+)$ value for the $N=80$ isotones at ^{136}Ba is given in terms of the increasing single-hole energy of the $h_{11/2}$ neutron configuration as the proton subshell is filled. The angular momentum transfer to the binary fragments in the reaction has also been investigated in terms of the average total γ-ray fold versus the scattering angle of the recoils.

DOI: 10.1103/PhysRevC.69.024316 PACS number(s): 21.10.Pc, 21.10.Tg, 27.60.+j

I. INTRODUCTION

Nuclei in the vicinity of the doubly closed-shell nucleus $^{132}_{50}Sn_{82}$ [1] give information on the basic single-particle structure and interactions between pairs of nucleons occupying the valence states. In particular, the evolution of structure in the $N=80$ isotones can be used to identify the pertinent role of the unnatural-parity $h_{11/2}$ neutron orbital which has a major influence on the makeup of the high-spin states in this region. Isomeric $I^{\pi}=10^+$ states have been reported in all the even-A $N=80$ isotones from $^{130}_{50}$Sn up to $^{148}_{68}$Er [2–7], with the exception of the $Z=56$ isotone, ^{136}Ba. In the recent paper by Genevey *et al.* [3] the significant reduction of the $B(E2)$ between the yrast 10^+ isomeric state and the first 8^+ state in the $Z\geqslant 58$ $N=80$ isotones [4–7] compared to their $Z\leqslant 54$ counterparts [2,3] has been discussed in terms of a significant component of the neutron $(\nu h_{11/2})^{-2}$ configuration in the wave function of the 8^+ state in the lighter systems.

The magnetic moment measurements of the yrast $I^{\pi}=10^+$ isomers in $^{138}_{58}$Ce and $^{140}_{60}$Nd [5] are all consistent with near-spherical, maximally aligned two-neutron-hole $(\nu h_{11/2})^{-2}$ configurations. Similarly, two-neutron-hole 10^+ states have also been observed in the lighter barium isotopes $^{132}_{56}$Ba [8] and $^{134}_{56}$Ba [9]. The differing structure of the 10^+ isomeric state with the structure of the 8^+ state seems the reason for the sudden decrease in the $B(E2:10^+\rightarrow 8^+)$ value for $Z>56$.

In the present paper we report on the structure of the stable nucleus $^{136}_{56}Ba_{80}$ studied using deep-inelastic reactions and time-correlated γ-ray spectroscopy. This completes the systematics of the even-Z $N=80$ isotones, with the observation of the "missing" (10^+) isomer in this nucleus, which has a tentative $(\nu h_{11/2})^{-2}_{10^+}$ configuration.

During the preparation of this manuscript, we became aware of a parallel study of $^{136}_{56}$Ba by Gan *et al.* [10], the results of which are consistent with those presented in the current work.

II. EXPERIMENTAL PROCEDURE

Prior to this study the medium-to-high-spin data on ^{136}Ba were restricted due to the β-stable nature of ^{136}Ba, which makes it difficult to populate with heavy-ion induced fusion-evaporation reactions. The $N=80$ isotone lies between the lighter barium isotopes which can be readily populated using this method [11] and heavier, neutron-rich isotopes which have been studied as residues from spontaneous fission

*Corresponding author. FAX:+44(0)1483-686781. Email address: j.valiente-dobon@surrey.ac.uk

[12–14]. To date, the data on the near-yrast states in ^{136}Ba come from work using β decay [15], (n,γ) reactions [16], Coulomb excitation [17], and light-ion (^{9}Be) induced fusion reactions [18]. As a result, prior to this work, the highest spin state known was the yrast 8^+ state identified by Dragulescu *et al.* [18].

The current work utilized a thin-target heavy-ion binary reaction to populate the medium-spin yrast states in ^{136}Ba. The experiment reported in the current work was performed at Lawrence Berkeley National Laboratory using an 850 MeV $^{136}_{54}$Xe beam provided by the 88 in. cyclotron incident on a self-supporting 420 μg cm^{-2} $^{198}_{78}$Pt target, isotopically enriched to $>$92%. The typical beam intensity was $\approx$1 pnA and the cyclotron beam had a natural micropulsing period of 178 ns. Reaction γ rays were detected using the GAMMASPHERE γ-ray array [19], which in this experiment consisted of 103 Compton-suppressed germanium detectors, 70 of which are electrically segmented into two D-shaped halves to improve the Doppler correction. The heavy-metal collimators from the bismuth germanate (BGO) suppression shields were removed thereby allowing a measurement of γ-ray fold to be taken for each event (see later). The Chico gas-filled parallel plate avalanche chamber ancillary detector [20] was used in combination with GAMMASPHERE to measure the angles (both polar and azimuthal) and the time-of-flight difference (ΔTOF) between the detection of both recoils, thus allowing an event-by-event Doppler shift correction to be made for emitted γ rays.

The experimental master trigger condition required two Chico elements and at least three germanium detectors in mutual coincidence. The hardware master-gate timing condition was set such that the third (and any subsequent) germanium signals in that event could be delayed by up to 670 ns with respect to the detection of the binary reaction fragments and the first two γ rays. Approximately 10^9 such events were recorded on tape during the course of the four-day experiment.

III. DATA REDUCTION AND OFF-LINE ANALYSIS

The beam-like and target-like fragments (BLFs and TLFs, respectively) were detected using Chico in coincidence with the γ rays emitted by the reaction product nuclei. The ΔTOF measured between the detection of the two fragments, together with the angular information given directly by the recoil detector, allowed the separation of the TLFs and BLFs (as shown in Fig. 1). The most intense region for the fragment distributions was observed at the grazing angle [21], which for this particular reaction occurred at approximately the same laboratory angle of 50° for both the TLFs and BLFs. Note that in the current work, there was also an experimental detection cutoff for $\theta<20°$ as a result of a mask which was introduced to cut the high counting rate in Chico at very forward angles. The reduction in counts in the particle identification spectrum at 60° occurs as a result of a support rib in the pressure window of Chico and was used as an internal calibration for the particle angular determination.

In the off-line analysis a software requirement was defined to include only events where at least three prompt γ rays occurred within ±15 ns of the binary fragments being detected in Chico. This allowed a well-defined time reference for all delayed γ rays decaying from isomeric states in the binary fragments to be used in the subsequent analysis. Figure 2(a) shows the sum of time distributions associated with the individual GAMMASPHERE detectors and Fig.

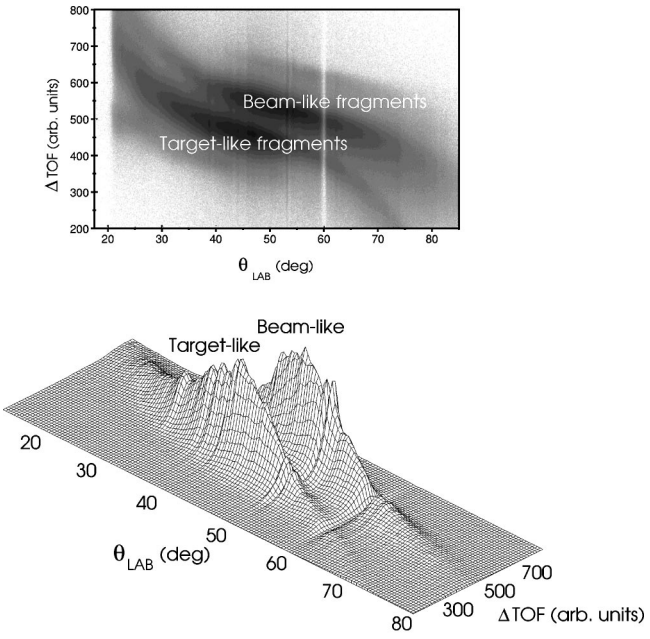

FIG. 1. Particle identification plot for the current work. The measurement of the ΔTOF and scattering angles of the recoils θ allows the two binary partners to be cleanly separated.

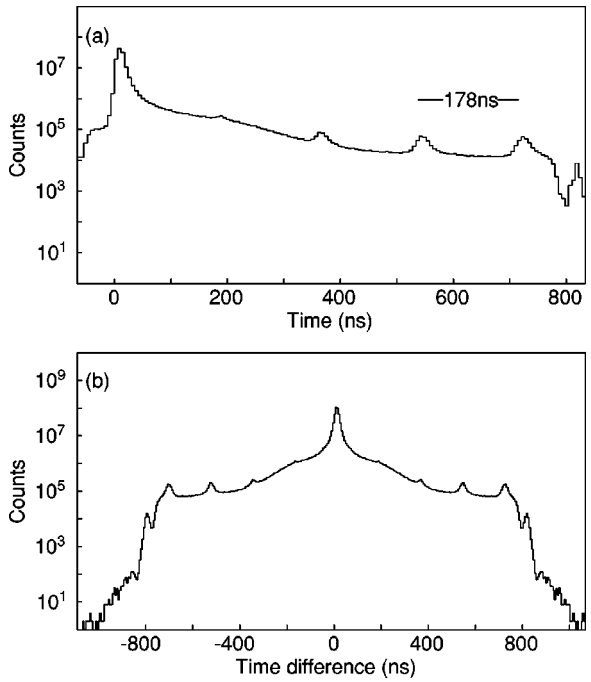

FIG. 2. Upper spectrum (a) shows the total time projection of γ-ray events in the current work, note that the time between the cyclotron bursts is 178 ns. Lower spectrum (b) shows the time difference between pairs of γ rays $(t_{\gamma_1}-t_{\gamma_2})$.

2(b) shows the relative time differences between γ rays measured in coincident events. By setting software gates on these spectra, specific temporal regions could be defined, corresponding to either prompt γ rays which were emitted from the fragments in flight or those decays from isomeric states in nuclei which were stopped in Chico.

The recoiling products stopped in Chico, which was $\approx$13 cm from the target position, corresponding to fragment times of flight of $\approx$4–15 ns. Due to the absence of hevimet collimators on GAMMASPHERE these stopped binary fragments were in the line of sight for the majority of GAMMASPHERE detectors, and thus decays from isomeric states with lifetimes ranging from nanoseconds to microseconds were observed with an efficiency that was approximately equal to that for γ rays emitted at the target position [20].

The maximum velocities of the binary partners were $\beta \approx 11\%$, as determined from the two-body kinematics of the reaction. Therefore, the prompt γ rays emitted in flight were heavily Doppler shifted. However, it was possible to correct the prompt γ-ray energies for the Doppler effect on an event-by-event basis using the interaction position of the recoils as measured by Chico. The interaction position determined the velocities β_{BLF} and β_{TLF} of the recoiling beam and target nuclei, respectively. By conservation of linear momentum [20] and assuming the limiting case of no particle evaporation,

$$P_{BLF,TLF} = \frac{P_0 \sin(\theta_{TLF,BLF})}{\sin(\theta_{BLF} + \theta_{TLF})}, \tag{1}$$

where $P_{BLF} = m_{(^{136}\mathrm{Xe})}\beta_{BLF}c$ and $P_{TLF} = m_{(^{198}\mathrm{Pt})}\beta_{TLF}c$ are the momenta of the recoiling beam and target nuclei, respectively; θ_{BLF} and θ_{TLF} are the laboratory scattering angles of the recoiling beam and target nuclei, respectively, and P_0 is the momentum of the incident beam. Note that since it is not possible to determine the mass of the recoils with Chico, the momenta of the recoils are calculated assuming the beam ^{136}Xe and target ^{198}Pt masses.

The Doppler-shifted γ rays were corrected according to [22]

$$E_S = E_0 \frac{\sqrt{1-\beta^2}}{1 - \beta \cos\Theta}, \tag{2}$$

where E_0 is the energy in the rest frame of the nucleus and Θ is the emission angle relative to the trajectory of the nucleus in the laboratory frame. The angle Θ was determined using the expression

$$\cos\Theta = \sin\theta_R \sin\theta_\gamma(\cos\phi_R \cos\phi_\gamma + \sin\phi_R \sin\phi_\gamma) + \cos\theta_R \cos\theta_\gamma, \tag{3}$$

where θ_R and ϕ_R are the scattering angles of the recoils (BLFs and TLFs), and θ_γ and ϕ_γ are the detection angles of the γ rays from GAMMASPHERE.

The γ-ray energies as measured in the laboratory frame could thus be Doppler corrected for either BLFs or TLFs. Note that in each case only the γ rays emitted by the nuclei for which the Doppler correction was made were enhanced in the resulting spectrum, while those with the incorrect Doppler correction were smeared out (see Fig. 3).

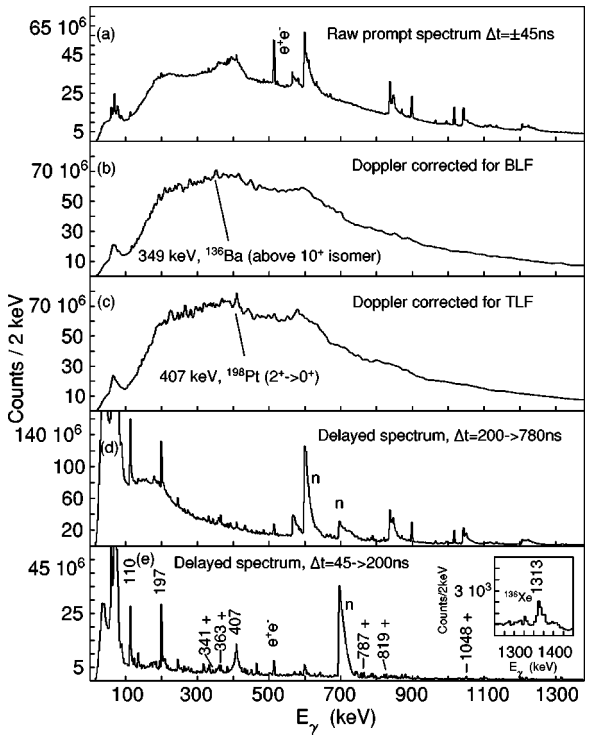

FIG. 3. Upper spectrum (a) shows prompt γ rays without any Doppler correction, spectra, (b) and (c) show the total projection of prompt Doppler corrected spectra for BLFs and TLFs, respectively. The lower two panels show delayed spectra for two different time ranges. Spectrum (d) shows delayed γ rays emitted within the time range 200–780 ns, while spectrum (e) shows γ rays emitted within the first 200 ns following the detection of fragments in Chico. The peaks marked with a "+" symbol are γ rays emitted during the deexcitation decay of the (10^+) isomer in ^{136}Ba.

Figure 3(a) shows the prompt γ rays which were measured to be within $\Delta t = \pm 45$ ns of the master trigger, with no Doppler correction applied. Figures 3(b) and 3(c) show the same spectra Doppler corrected for BLFs and TLFs, respectively. Note that the BLF Doppler corrected spectrum [Fig. 3(b)] shows the prompt 349 keV transition which feeds the (10^+) isomer in ^{136}Ba (see later), while in the TLF Doppler corrected spectrum the 407 keV transition $(2^+ \rightarrow 0^+)$ in ^{198}Pt [23] can be identified. The low-lying prompt transitions from the ^{136}Xe beam nucleus [e.g., $E(2^+ \rightarrow 0^+) = 1313$ keV] are not obviously evident in Fig. 3(b) due to the presence of a low-lying $I^\pi = 6^+, t_{1/2} = 3$ μs isomeric state in this nucleus [24], which traps most of the prompt feeding.

Figures 3(d) and 3(e) show delayed γ rays gated in two different time regimes. Figure 3(d) shows γ rays emitted within the time range 200 ns–780 ns, while Fig. 3(e) shows γ rays within the first 200 ns of the detection of the binary fragments in Chico. The latter shows transitions associated with the low-lying states of ^{136}Ba [16] (see later), the $2^+ \rightarrow 0^+$ in ^{198}Pt (407 keV), and the delayed neutron peaks at 596 keV and 691 keV coming from neutron excitations of ^{74}Ge and ^{72}Ge, respectively. The two very intense peaks at 110 keV and 197 keV are due to the γ decay of the $\frac{5}{2}^+$ state

TABLE I. Summary of the different matrices and cubes used in the analysis of the present work.

ID	Description	Time gate [Δt(ns)]			Additional conditions
		x axis	y axis	z axis	
I	γ-γ delayed matrix	45→780	45→780		
II	γ-γ-*time* cube				$t_{\gamma_1}-t_{\gamma_2}=5$ ns (see Fig. 2)
III	$\gamma_{delayed}$-γ_{prompt}-Δt cube[a]	45→780	±45		γ_{prompt} gated on BLF
IV	γ-γ prompt matrix[b]	±45	±45		341, 363, 787, 819, 1048 (keV)[c]
V	$\gamma_{delayed}$-γ_{prompt}	45→780	±45		γ_{prompt} gated on BLF
VI	$\gamma_{delayed}$-θ_{scatt}-*fold* cube[d]	45→780			

[a] Δt is defined as $t_{delayed}-t_{prompt}$.
[b] Doppler corrected for BLF.
[c] Delayed γ rays in ^{136}Ba.
[d] θ_{scatt} is the scattering angle of the BLF measured by Chico.

in ^{19}F, with a half-life $t_{1/2}=89.3$ ns [23], which is used in the electrical segmentation process of the HPGe detectors.

The full analysis of these data required a number of different coincidence matrices and cubes to be sorted. These were subsequently analyzed using the RADWARE and ANA packages [25,26]. Those of relevance to the present work are listed in Table I.

IV. EXPERIMENTAL RESULTS

A wide range of isomeric states with half-lives in the nanosecond-to-microsecond range were populated in both the xenon and platinum regions. Background subtracted γ-ray spectra and their measured half-lives for isomers populated in the beam-like and the target-like regions are shown in Figs. 4 and 5, respectively. The half-lives have been fitted with a constant background in addition to the exponential decay curve. Table II summarizes these half-life measurements. The consistency between the literature values and those of the current work shows the reliability of this analysis. Note that the isomers found in ^{131}I, ^{133}I, ^{184}W, ^{191}Os, ^{192}Os, and ^{198}Pt have not been reported in the literature prior to the current work.

The main focus of this paper is the identification of the internal structure of $^{136}_{56}$Ba which corresponds to the addition of two protons and the removal of two neutrons from the $^{136}_{54}$Xe projectile. The level scheme deduced from the present work for ^{136}Ba is shown in Fig. 6 and was obtained by examining background subtracted spectra from (i) an out-of-beam matrix, constructed from delayed γ-γ coincidences

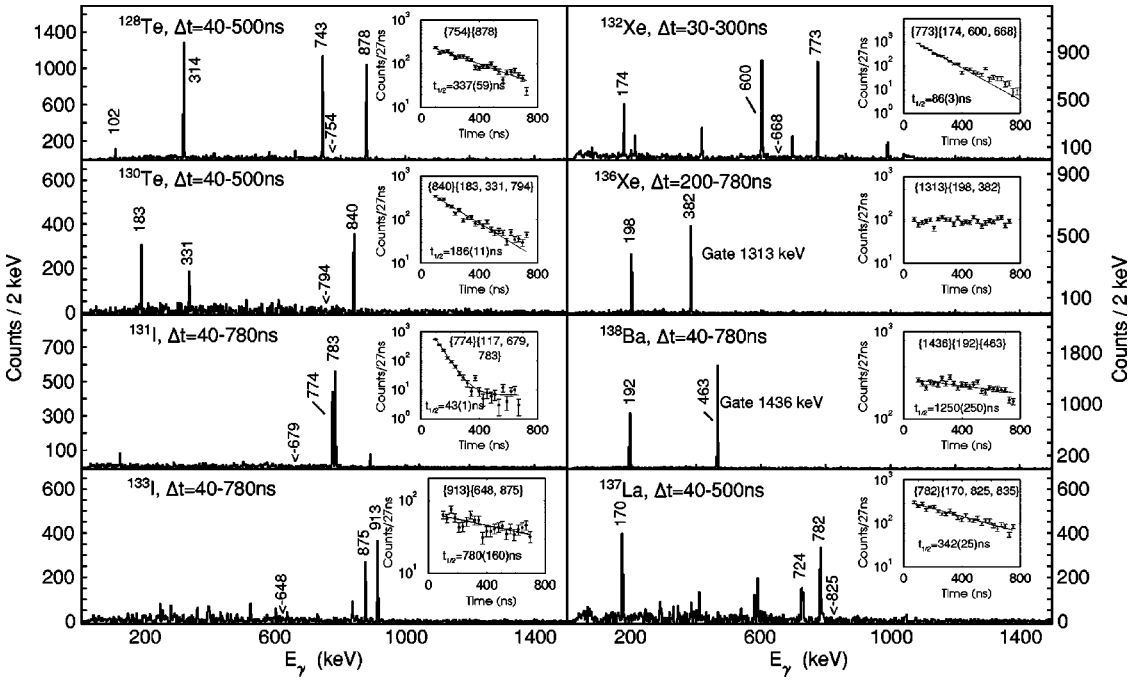

FIG. 4. Background subtracted γ-ray spectra for selected isomeric states in BLFs populated by a ^{136}Xe beam at 850 MeV impinging on a ^{198}Pt target. The insets show the fitted half-life curves obtained in this work and the pairs of double γ-ray gates used to obtain the half-life curve are given in braces. The isomers identified in ^{131}I and ^{133}I have not previously been reported.

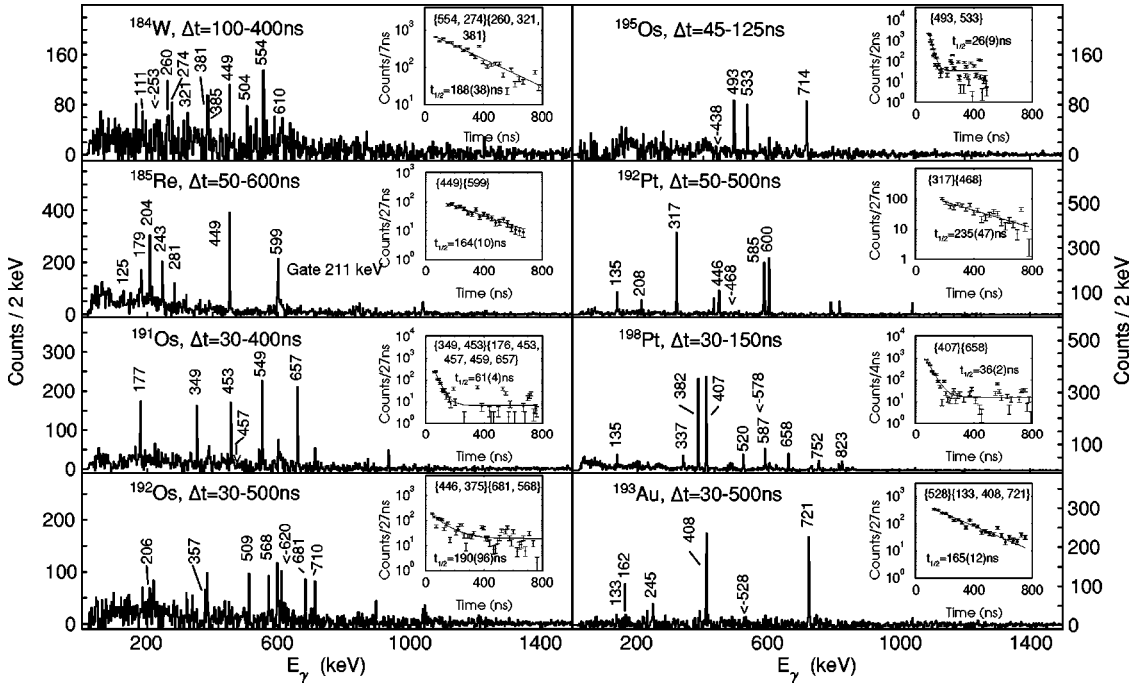

FIG. 5. Background subtracted γ-ray spectra for selected isomeric states in TLFs populated by a ^{136}Xe beam at 850 MeV impinging on a ^{198}Pt target. The insets show the fitted half-life curves obtained in this work and the pairs of double γ-ray gates used to obtain the half-life curve are given in braces. The isomers identified in ^{184}W, ^{191}Os, ^{192}Os, and ^{198}Pt have not previously been reported.

(see Table I) for the levels below the (10^+) isomer; (ii) an in-beam prompt matrix, constructed from γ-γ coincidences gated on delayed transitions in ^{136}Ba and Doppler corrected for the BLFs (see Table I) [this enabled the identification of prompt transitions which feed the (10^+) isomer]; (iii) a prompt-delayed matrix which corresponded to pairs of γ rays in which the first one came as a prompt, in-flight decay, while the delayed transition was measured between 45 and 780 ns later (see Table I).

TABLE II. Measured half-lives of selected isomers observed in the present work and a comparison with literature values. Previously unreported isomers have been identified in ^{131}I, ^{133}I, ^{184}W, ^{191}Os, ^{192}Os, ^{198}Pt.

Isotope	I^π	E_x (keV)	$t_{1/2}$(ns)	
			Current work	Previous works
^{128}Te	10^+	2791	337±59	370±30 [36]
^{130}Te	(7^-)	2146	186±11	115±8 [27]
^{131}I		2352	43±1	
^{133}I		2436	780±160	
^{132}Xe	7^-	2214	86±3	90±10 [28]
^{136}Xe	6^+	1892	>1000	3000±300 [24]
^{138}Ba	6^+	2091	1250±250	800±100 [29]
^{137}La	$\frac{19}{2}^-$	1870	342±25	360±40 [30]
^{184}W	15^-	3714	188±38[a]	
^{185}Re	$\left(\frac{21}{2}^-\right)$	2124	164±10	120±15 [32]
^{191}Os		2640	61±4	
^{192}Os		4115	190±96	
^{195}Os	$\left(\frac{27}{2}^-\right)$	2229	26±9	26±2 [33]
^{192}Pt	(10^-)	2172	235±47	250±30 [34]
^{198}Pt		3019	36±2	
^{193}Au	$\frac{31}{2}^+$	2486	165±12	150±50 [35]

[a]A detailed study of this isomer can be found in Ref. [31].

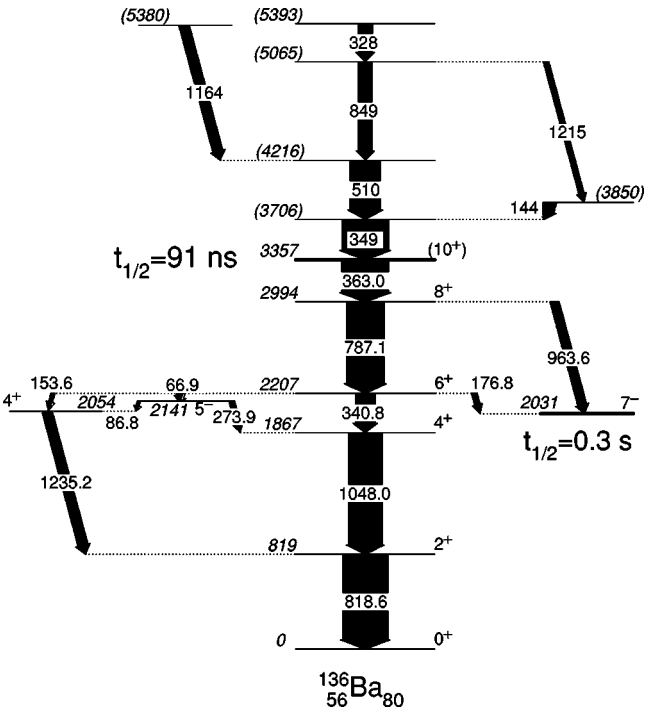

FIG. 6. Level scheme of ^{136}Ba deduced from the present work with the 91±2 ns $I^\pi=(10^+)$ isomer. The widths of the arrows are proportional to the relative γ-ray intensities.

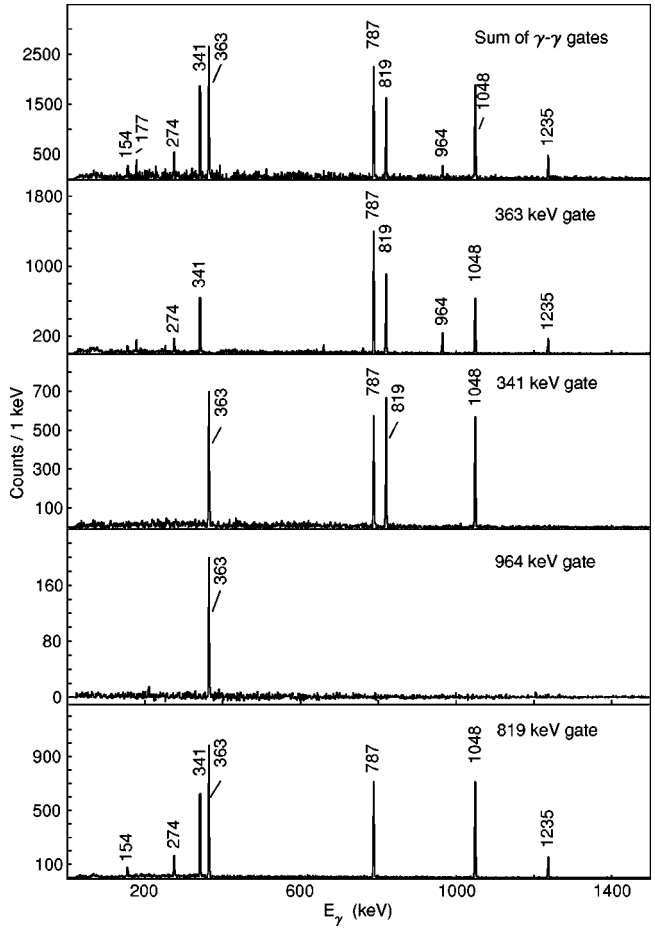

FIG. 7. Background subtracted delayed γ-ray spectra from the decay of the 10^+ isomer in ^{136}Ba. The time condition is that the γ rays are observed in the time range $\Delta t = 100-600$ ns with respect to the master trigger.

A. Transitions below the (10^+) isomer in ^{136}Ba

The observation of the 819 keV $(2^+ \rightarrow 0^+)$ transition in ^{136}Ba in the delayed spectrum shown in Fig. 7 clearly demonstrates the presence of an isomer in this nucleus. Figure 7 shows all the transitions up to the previously reported 8^+ state, together with a transition at 363 keV, which we interpret to be the direct decay from a (10^+) isomer. The excitation energy of this isomer is established from the γ-γ coincidence relationships to be 3357 keV.

Spins and parities have been established for the levels in ^{136}Ba up to the $I^\pi = 8^+$ state at 2994 keV [16,18]. The $I^\pi = 8^+$ [18] state at 2994 keV which decays to the $I^\pi = 6^+$ state via a γ ray of energy 787 keV is clearly observed in the present work together with a previously unreported branch which decays to the $I^\pi = 7^-$ isomeric state at 2031 keV [16] via a 964 keV transition.

The multipolarity of the 363 keV transition could be $E1, E2$, or $M1$, from intensity balancing across the 2994 keV state. Assignments of $8^\pm$ and 9^- can be ruled out for the 3357 keV level on the basis of nonobservation of direct decay branches to the 6^+ state at 2207 keV and to the 7^- isomeric state at 2031 keV. Spins of 11 and higher for the state can be ruled out on the basis of the electron conversion associated with such high-multipole decays and the measured intensity balance across the 2994 keV state. Of the remaining spin/parity assignments 9^+ and 10^+, the (10^+) is strongly favored on the basis of both the systematics of the even-Z $N=80$ isotones and the shell-model calculations (see later).

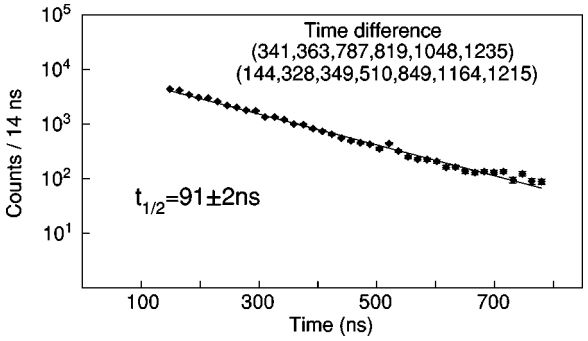

FIG. 8. Time difference γ-γ spectrum obtained by gating above and below the isomeric 10^+ state to determine the half-life of the 10^+ state in ^{136}Ba(91±2 ns).

A half-life of $t_{1/2} = 91 \pm 2$ ns, see Fig. 8, was obtained for the decay of the (10^+) state by measuring the time difference between prompt and delayed transitions feeding in and out of the proposed (10^+) state. Assuming an electric quadrupole nature for the 363 keV transition, the $B(E2: 10^+ \rightarrow 8^+)$ for ^{136}Ba is calculated to be $0.97 \pm 0.2\ e^2\ \text{fm}^4 = 0.0231 \pm 0.0005$ W.u. Figure 9(a) shows the delayed transitions below the isomer, gated on the prompt 144, 328, 349, and 510 keV transitions in ^{136}Ba (see later). The energies and intensities of the delayed transitions observed in ^{136}Ba are given in Table III.

B. Transitions above the (10^+) isomer in ^{136}Ba

Prompt transitions which form a cascade feeding into the proposed $I^\pi = (10^+)$ isomer were deduced using a γ-γ prompt

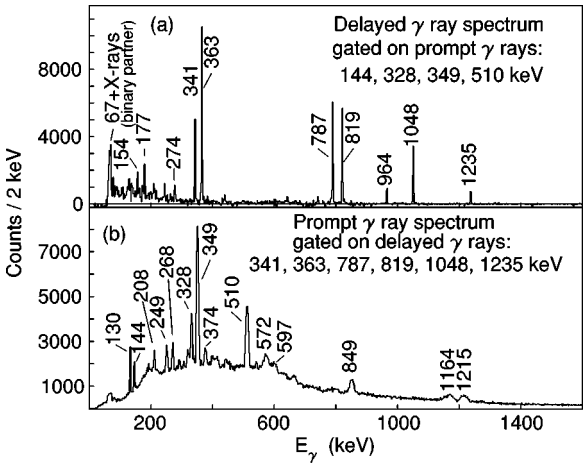

FIG. 9. Upper spectrum (a) shows the background subtracted delayed γ-ray spectrum gated by prompt transitions above the proposed 10^+ isomer. Lower spectrum (b) shows the background subtracted prompt γ-ray spectrum gated by delayed transitions placed below the proposed 10^+ isomer.

TABLE III. Energies, assignments, and relative out-of-beam intensities for transitions observed in $^{136}_{56}$Ba. The uncertainties in the transition energies are ±0.2 keV.

E_γ (keV)	E_i	E_f	I_i^π	I_f^π	I_γ (delayed)
66.9	2207	2141	6^+	5^-	70(4)
86.8	2141	2054	5^-	4^+	33(7)
153.6	2207	2054	6^+	4^+	40(6)
176.9	2207	2031	6^+	7^-	67(5)
273.9	2141	1867	5^-	4^+	69(5)
340.8	2207	1867	6^+	4^+	242(10)
363.0	3357	2994	(10^+)	8^+	566(20)
787.1	2994	2207	8^+	6^+	460(20)
818.6	819	0	2^+	0^+	551(20)
963.6	2994	2031	8^+	7^-	112(11)
1048.0	1867	819	4^+	2^+	410(22)
1235.2	2054	819	4^+	2^+	126(12)
1312.0					15(3)

TABLE IV. Energies, assignments, and relative in-beam intensities for transitions observed in $^{136}_{56}$Ba above the (10^+) isomer. The energy resolution for prompt γ rays is ≈1%.

E_γ (keV)	E_i	E_f	I_i^π	I_f^π	I_γ (prompt)
130					598(24)
144	(3850)	(3706)			332(15)
208					109(8)
249					110(6)
268					94(5)
328	(5393)	(5065)			176(9)
349	(3706)	(3357)		(10^+)	566(10)
374					94(5)
510	(4216)	(3706)			372(10)
849	(5065)	(4216)			166(8)
1164	(5380)	(4216)			126(9)
1215	(5065)	(3850)			121(9)

matrix Doppler corrected for BLFs and single-gated by the yrast delayed γ rays observed below the isomer in ^{136}Ba (see Table I). Figure 9(b) shows the prompt transition above the isomer, gated on the delayed 341, 363, 787, 819, 1048, and 1235 keV transitions in ^{136}Ba. Figure 10 shows a selection of coincidence spectra for γ rays above the isomer. The energies and intensities of the prompt transitions observed above the isomer are given in Table IV.

The prompt γ-γ coincidence spectra for states above the (10^+) isomer show evidence for a cascade involving the 349, 510, 849, and 328 keV transitions which are mutually coincident. The ordering of these transitions above the isomer is based on the intensity measurements and the identification of a side-feeding transition with an energy of 1164 keV which is in prompt coincidence with the 349 and 510 keV transitions and appears to bypass the higher-lying members of the cascade. The crossover branch associated with the 144 and 1215 keV γ rays appears to feed directly into the proposed 3706 keV level which is depopulated by the 349 keV transition. The ordering of the 144 keV and 1215 keV transitions is established in the current work on the basis of measured γ-ray intensity.

The ordering of the structure built on top of the (10^+) isomeric state as presented in the current work is tentative. Specifically, the intense transition at 130 keV is in mutual coincidence with the cascade of 349, 510, 849, and 328 keV (see Fig. 10), although it does not appear to be in coincidence with the 1164 keV transition which is assumed to feed into the proposed level at 4216 keV. This situation suggests that the 130 keV transition lies above the 849 and 1215 keV transitions, but the large, measured γ-ray intensity for the 130 keV line (see Table IV) presents a potential problem. If it is placed above the proposed 5065 keV level, not all of the

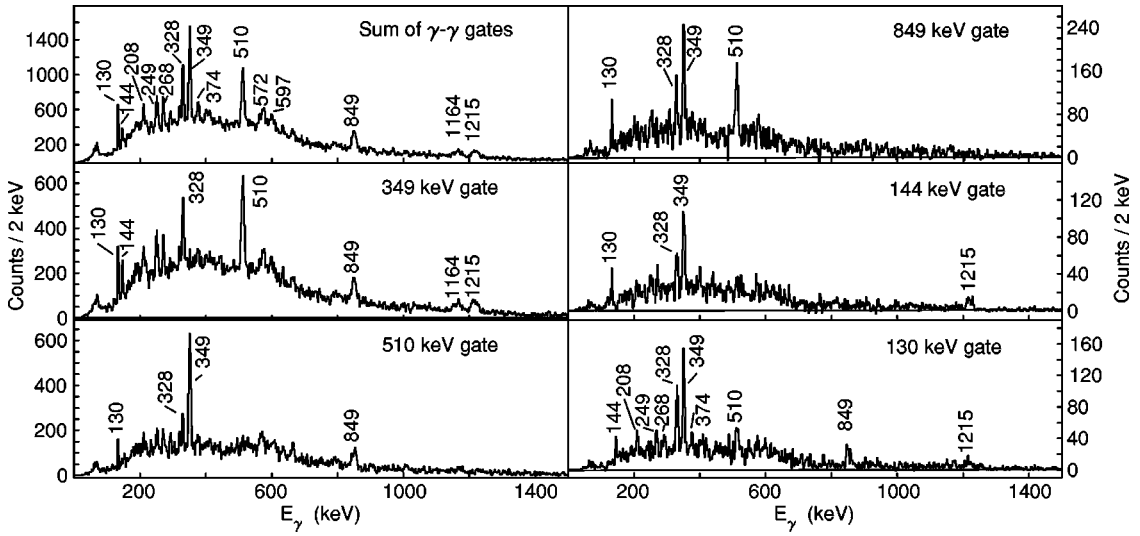

FIG. 10. Background subtracted prompt γ-ray spectra single-gated by the delayed 341, 363, 787, 819, 1048, and 1235 keV transitions placed below the (10^+) isomer in ^{136}Ba. The time condition is that the prompt γ rays are observed within $\Delta t = \pm 45$ ns of the master trigger.

decay flux can be accounted for in the present work and other nonobserved decay branches for the decay flux must be present. We note that the 130 keV transition is in coincidence with the unplaced lines at 208, 249, 264, and 130 keV, which may account for some of this missing intensity. While the quality of the spectra used for the prompt γ-γ coincidences above the (10^+) isomer can demonstrate a number of mutual coincidences (see Fig. 10), they are not of sufficient statistical significance to preclude a different ordering of the lines above the (10^+) isomer. One alternative could be that the 130 keV line lies lower in the cascade, i.e., either directly feeding into the isomeric state or into the proposed level at 5393 keV.

V. DISCUSSION

The nucleus $^{136}_{56}$Ba has six valence protons outside the closed shell $Z=50$ and two-neutron holes with respect to the closed shell $N=82$. It was pointed out in 1973 by Meyer-Lévy and Lopac [37] that many of the low-lying properties of the $N=80$ isotones might be explained by the simple coupling of the two-neutron holes to a quadrupole vibrator core. The authors of Ref. [37] also noted that the spectral pattern of the $N=80$ isotones from $^{132}_{52}$Te up to $^{140}_{60}$Nd were rather similar with the presence of a two-phonon quadrupole vibrational triplet established for ^{136}Ba and its neighbor, ^{138}Ce. This work ignored any effects from the proton particles and allowed couplings of neutron-hole states from the $d_{3/2}, s_{1/2}, h_{11/2}, d_{5/2}$, and $g_{7/2}$ orbitals to a vibrational core. While this approach gave a reasonable prediction for the energies of the low-lying negative-parity states and the first 2^+ and 4^+ levels, it predicted that the yrast 6^+ and 8^+ states lay above the yrast 10^+ level. This clearly pointed to the need to include *both* proton and neutron degrees of freedom in the calculations for such apparently simple, two-neutron-hole systems.

A. Shell-model and pair-truncated shell-model calculations

In order to understand the structure of ^{136}Ba, a shell-model approach such as the one described in Ref. [38] has been carried out in the present work. To truncate the model space, the proton single-particle orbitals involved in the calculations are restricted to the three orbitals $0g_{7/2}, 1d_{5/2}$, and $0h_{11/2}$, which have initial single-particle energies of 0.0, 0.963, and 2.760 MeV, respectively. The neutron single-hole orbitals include all of the five orbitals between the $N=50$ and 82 shell, i.e., the $1d_{3/2}, 0h_{11/2}, 2s_{1/2}, 1d_{5/2}$, and $0g_{7/2}$ which have single-hole energies of 0.0, 0.242, 0.332, 1.655, and 2.434 MeV, respectively. Those single-hole energies are extracted from experiment.

The effective shell-model Hamiltonian is written as

$$H = H_\nu + H_\pi + H_{\nu\pi}, \tag{4}$$

where H_ν, H_π, and $H_{\nu\pi}$ represent the neutron-neutron interaction, the proton-proton interaction, and the neutron-proton interaction, respectively. The interaction among like nucleons H_τ ($\tau=\nu$ or π) consists of spherical single-particle energies, a monopole-pairing interaction, a quadrupole-pairing

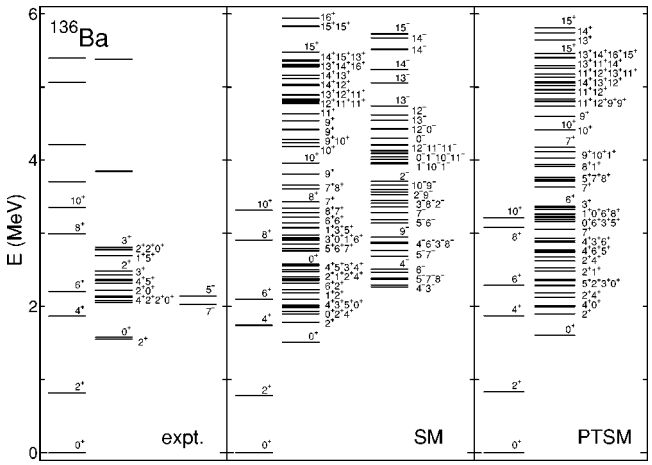

FIG. 11. Comparison of the experimental energy spectra (left panel) with the results of the shell-model calculation (middle panel) and the pair-truncated shell-model calculations (right panel) for ^{136}Ba (see text for details). Note that in the middle and right panels the states are separated into columns for the yrast states up to 10^+, the positive-parity states and the negative-parity states.

(QP) interaction, a quadrupole-quadrupole (QQ) interaction, a (HP) hexadecapole-pairing, and a (HH) hexadecapole-hexadecapole interaction. The strengths of these interactions are determined so as to reproduce the corresponding experimental energies of the singly closed-shell nuclei $^{138}_{56}Ba_{82}$ and $^{130}_{50}Sn_{80}$. A quadrupole-quadrupole interaction is the only term in $H_{\nu\pi}$, the strength of which is adjusted to reproduce the excitation energy of the 10^+ isomer. A detailed description of these interactions can be found in Ref. [38]. The determined strengths of the interactions, in MeV, are $G_{0\nu}=0.145, G_{2\nu}=0.016, k_\nu=0.035, G_{4\nu}=0.700, k_{4\nu}=1.600, G_{0\pi}=0.180, G_{2\pi}=0.010, k_\pi=0.055, G_{4\pi}=0.600, k_{4\pi}=0.300$, and $\kappa_{\nu\pi}=-0.165$. The definitions of the HP and HH interactions are extensions of the QP and the QQ interactions from angular momentum coupling two to four, but no radial dependence is assumed. These hexadecapole interactions are necessary for a better fit, since the number of valence protons and neutrons is small in ^{136}Ba and quadrupole collectivity is still not dominant compared to other interactions. In the central panel of Fig. 11 the results of the shell-model calculations are shown compared with the experimental decay scheme for ^{136}Ba as deduced in the current work. The comparison for the even-spin yrast sequence up to the proposed (10^+) isomer is rather impressive, with the calculations reproducing the ordering of these levels.

To study the basic structure of the levels in ^{136}Ba and to keep the basis to a reasonable truncation, the pair-truncated shell-model (PTSM) approach, which is described in Ref. [39], has also been used. This approach is very similar to the interacting boson model in concept, but the bosons are now replaced by correlated nucleon pairs to treat Pauli effects explicitly. In addition to the $S:J=0$ pairs, the truncated valence space only allows pair excitations of the following type, $D:J=2, G:J=4$ and H. Note that the calculation is limited to a single H pair that can only be formed by the coupling of two $h_{11/2}$ proton particles or neutron holes to angular

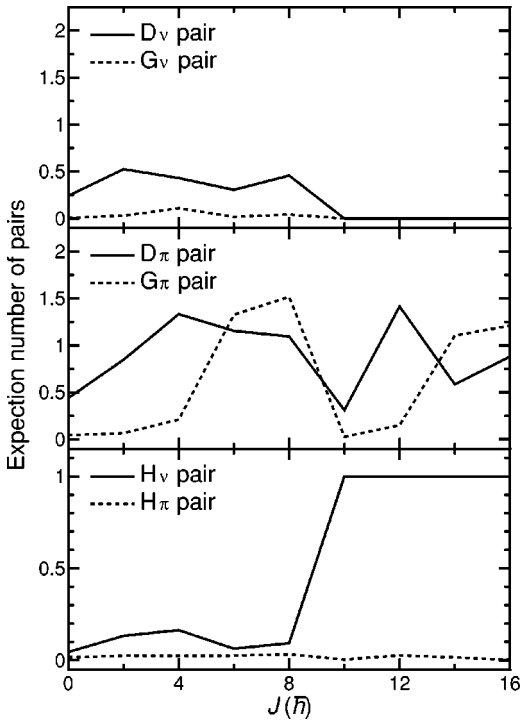

FIG. 12. The upper panel shows the expectation numbers of neutron D_ν and G_ν pairs, the middle panel shows the expectation numbers of proton D_π and G_π pairs calculated in the PTSM. The lower panel shows the expectation numbers of neutron and proton $H_{\nu,\pi}$ pairs calculated in the PTSM. The expectation numbers are for the positive yrast states.

momentum $J=0,2,4,6,8,10$. In contrast, the other pairs in this model space are collective and can be made from linear combinations of other angular momentum couplings between pairs of nucleons in different single-particle orbitals. All these pairs have positive parity so that only positive parity states are predicted. In the right panel of Fig. 11 the results of the PTSM are shown in comparison with the shell-model and experimental results.

Figure 12 shows the expectation number of pairs for the yrast positive-parity sequence in ^{136}Ba from the PTSM calculations. From the upper two panels in Fig. 12, one can see that the predicted wave functions of the positive-parity yrast states up to spin 8^+ are mostly dominated by proton D and G pair couplings. On the contrary, as shown in the lowest panel of Fig. 12, the yrast 10^+ state is dominated by a neutron H pair, corresponding to the maximally coupled $(\nu h_{11/2})^{-2}$ configuration. The dramatic alteration in the number and character of pairs between the 10^+ isomeric state and the 8^+ state is responsible for the isomeric nature of the 10^+ state and also for the large reduction of $B(E2)$ transition rate (see below). The shell-model calculations (see Fig. 11) predict that a second 8_2^+ state lies just below the yrast (10^+) isomer. This is predominantly the nonmaximally coupled $(\nu h_{11/2})^{-2}_{8^+}$ configuration. As shown in Table V the wave function of the second 8_2^+ state is dominated by an H_ν pair meanwhile the yrast 8_1^+ state is dominated by D_π and G_π pairs.

Using the resultant shell-model wave functions, we can predict $B(E2)$ values using effective charges with the conventional relation $e_\nu=-\delta e$ and $e_\pi=1+\delta e$ as described in Ref. [40]. Note that the effective charge for the neutron is negative since neutrons are treated as holes in this scheme. The δ value is determined to give the experimental $B(E2:2_1^+ \rightarrow 0_1^+)$ value. The adopted effective charges are $e_\nu=-0.82e$ and $e_\pi=+1.82e$. The calculations predict a value for the decay from this isomer of $B(E2:10_1^+ \rightarrow 8_1^+)=0.04\ e^2\ \mathrm{fm}^4$ compared to the experimentally deduced result of $0.97(2)e^2\ \mathrm{fm}^4$. Table VI lists the calculated and experimental $B(E2)$ values for the yrast sequence in ^{136}Ba. Note that the theoretical staggering of $B(E2)$ values is caused by the alternation of the number of proton D pairs and G pairs and the neutron H pair.

TABLE V. The expectation numbers of D, G, and H pairs calculated in the PTSM for the yrast 8_1^+ state and the second 8_2^+ state.

J^π	D_ν	G_ν	H_ν	D_π	G_π	H_π
8_1^+	0.4577	0.0431	0.0938	1.0948	1.5163	0.0331
8_2^+	0.0012	0.0068	0.9911	0.2213	0.0272	0.0043

The shell-model calculations also predict the observed low-lying negative-parity states with spin/parity 5^- and 7^-, and intriguingly also predict an 8^- state at a similar energy. There is no evidence for the 8^- negative-parity yrast trap in the current data. Such a state might however be very long lived, particularly if it lies below the well-known $t_{1/2}=0.3$ s $I^\pi=7^-$ isomer [23]. There is no evidence in the current work for the population of the second 2^+ state at 1551 keV corresponding to the $n=2$ phonon vibration [23].

With regard to the comparison between the calculations and the data for the states above the (10^+) isomer, it is noteworthy that the yrast states which are predicted to lie above the isomer all have negative parity and thus must be comprised partly from a $\nu h_{11/2}$ component in their wave function. Indeed the calculations do not predict a positive-parity state of spin 11 or higher until $\approx$1.5 MeV above the isomeric (10^+) state. However, the calculations predict a 10^- state which lies a few hundred keV above the (10^+) isomer and both 11^- and 12^- states a few hundred keV above that.

B. Comparison with $N=80$ isotones

All the even-Z $N=80$ isotones (see Fig. 13) from $^{130}_{50}$Sn to $^{148}_{68}$Er exhibit 10^+ isomeric states [2–7]. In $^{130}_{50}$Sn [2], $^{132}_{52}$Te

TABLE VI. Comparison of the yrast $B(E2)$ values in the shell model (SM) with the measured values in $e^2\ \mathrm{fm}^4$. The experimental data values have been taken from Refs. [41,42] and the present work.

$J_i^\pi \rightarrow J_f^\pi$	SM	Expt.
$2_1^+ \rightarrow 0_1^+$	802	801(6)
$4_1^+ \rightarrow 2_1^+$	1093	
$6_1^+ \rightarrow 4_1^+$	251	38.6(9)
$8_1^+ \rightarrow 6_1^+$	932	
$(10_1^+) \rightarrow 8_1^+$	0.04	0.97(2)

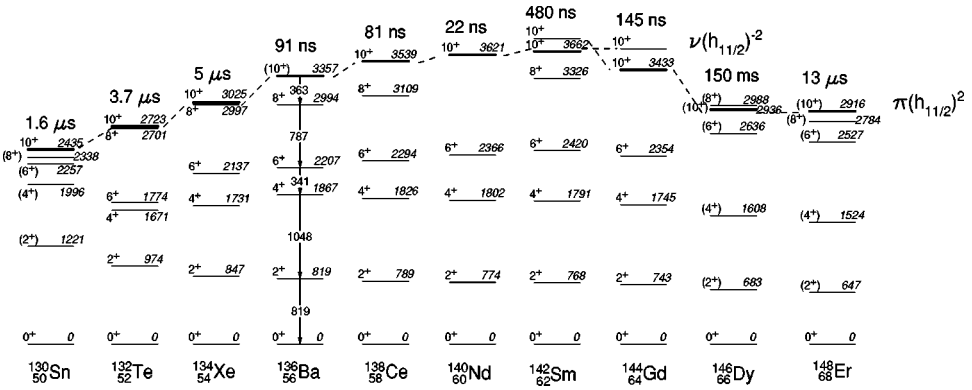

FIG. 13. Energy systematics for the $N=80$ isotones (see text for details).

[3], $^{134}_{54}$Xe [3], $^{138}_{58}$Ce [4], and $^{140}_{60}$Nd [5] this 10^+ isomer has been associated with a $(\nu h_{11/2})^{-2}_{10^+}$ configuration. In ^{138}Ce and ^{140}Nd [5] the magnetic dipole moment measurements yielding values of $g=-0.176(10)$ and $g=-0.192(12)$, respectively, suggest that the configurations for these two 10^+ isomers are consistent with the $(\nu h_{11/2})^{-2}_{10^+}$ configuration being the major component. In $^{142}_{62}$Sm and $^{144}_{64}$Gd [6], two 10^+ states have been observed with the lower-lying one being isomeric. This has been interpreted [6] as competing $(\nu h_{11/2})^{-2}$ and $(\pi h_{11/2})^2$ configurations. In $^{142}_{62}$Sm, the (lower-lying) isomeric 10^+ state is mainly two-neutron holes in the $h_{11/2}$ shell, meanwhile for $^{144}_{64}$Gd the isomeric 10^+ state is proposed to be mainly a two-proton configuration. For the heavier isotones $^{146}_{66}$Dy [7,43] and $^{148}_{68}$Er [7,44], the 10^+ isomeric states are both thought to have predominantly $(\pi h_{11/2})^2_{10^+}$ configurations, since according to the systematics the $(\nu h_{11/2})^{-2}$ states are expected to be around 3.7 MeV and have not been reported in these nuclei to date [7].

Figure 14(c) shows the systematics of the $B(E2:10^+ \rightarrow 8^+)$ for the even-Z $N=80$ isotones from ^{130}Sn to ^{142}Sm. There is an obvious retardation in the decay from the isomeric 10^+ state for ^{136}Ba, ^{138}Ce [4], and ^{142}Sm [6] compared to the lighter isotones. Lach *et al.* [6] suggest that such large hindrances require a high configuration forbiddenness and suggested a seniority four configuration for the yrast 8^+ state in ^{142}Sm.

The sudden decrease in the $B(E2:10^+ \rightarrow 8^+)$ value at ^{136}Ba as compared to the lighter $N=80$ isotones can be understood qualitatively in terms of the likely components of the wave functions of the yrast (10^+) and 8^+ states. As discussed above, from g-factor measurements and energy systematics, the nature of the yrast isomeric 10^+ state is predominantly of $(\nu h_{11/2})^{-2}$ character in all the even-Z $N=80$ isotones between ^{130}Sn and ^{142}Sm. For ^{130}Sn, the closed-shell nature of the $Z=50$ core gives rise to a "textbook" two-hole single-j shell multiplet, implying that the yrast 8^+ state has a $(\nu h_{11/2})^{-2}$ character. By a similar argument, the valence two-proton system $^{132}_{52}$Te can have only seniority two couplings in the $Z>50$ valence space used. Neglecting excitations into the proton $h_{11/2}$ orbitals (which is reasonable since these orbitals are at the top of the shell) the two valence protons alone could only generate a maximum angular momentum of 6^+ from $(\pi g_{7/2})^2$. Hence states of spin 8^+ or more must have seniority four, or incorporate the neutron pair with $J>0$, since breaking the $Z=50$ core would be energetically less favorable. For $Z>54$, however, an angular momentum of 8 and above can also be generated solely in the proton space. The development of an increasing proton component in the yrast 8^+ state would then explain the observed decrease in the $B(E2)$ from the predominantly two-neutron 10^+ state.

The smoothly increasing excitation energy of the 10^+ isomeric state [and by inference the $(\nu h_{11/2})^{-2}$ configuration] appears as a standard feature of the $N=80$ isotones from tin to samarium. This can be understood from Fig. 14(a), which shows the excitation energy of the lowest-lying $I^\pi=\frac{11}{2}^-$ single-hole state in the odd-A $N=81$ isotones. The single-hole excitation energy of the $h_{11/2}$ neutron orbital is observed to increase with proton number. This increase in single-hole energy is responsible for an increase of more than 1 MeV in the excitation energy of the yrast 10^+ state between $^{130}_{50}$Sn and $^{140}_{60}$Nd [see Fig. 14(b)]. This increased excitation energy means that the seniority four configurations which include the proton configurations can begin to compete energetically with the seniority two $(\nu h_{11/2})^{-2}_{8^+}$ configuration in the $N=80$ isotones at the barium isotone and for heavier elements. This results in a reduction of the $(\nu h_{11/2})^{-2}$ component in the wave function of the yrast 8^+ states, which in turn gives rise to the dramatic reduction in $B(E2:10^+ \rightarrow 8^+)$ value at ^{136}Ba.

VI. DETERMINATION OF ANGULAR MOMENTUM TRANSFER VIA THE STUDY OF γ-RAY FOLD

The knowledge of entry spin distributions and the related angular momentum population in deep-inelastic reactions has a significant bearing on the potential for using such mechanisms in the study of high-spin states in neutron-rich nuclei. While some effort was made in this area in the 1970s (e.g., Ref. [45]), there have been only limited recent studies which utilize the power of large-scale γ-ray arrays for channel selection in attacking this problem (e.g., Ref. [46]). In its full complement GAMMASPHERE has a total of 110 HPGe detectors all of which are Compton suppressed, i.e., each is surrounded by a high Z, high density oxide BGO shielding. This shielding improves the peak-to-total ratio by reducing the Compton background, but at the same time it can also be used to measure the γ-ray fold for each event.

The total fold F_{tot} measured in each event was the result of adding the following contributions (see Fig. 15):

$$F_{tot} = F_{BGO} + F_{HPGe} + F_{CS}, \tag{5}$$

where F_{BGO} is the number of counts detected per event in all the BGO shieldings, F_{HPGe} is the number of γ rays, not

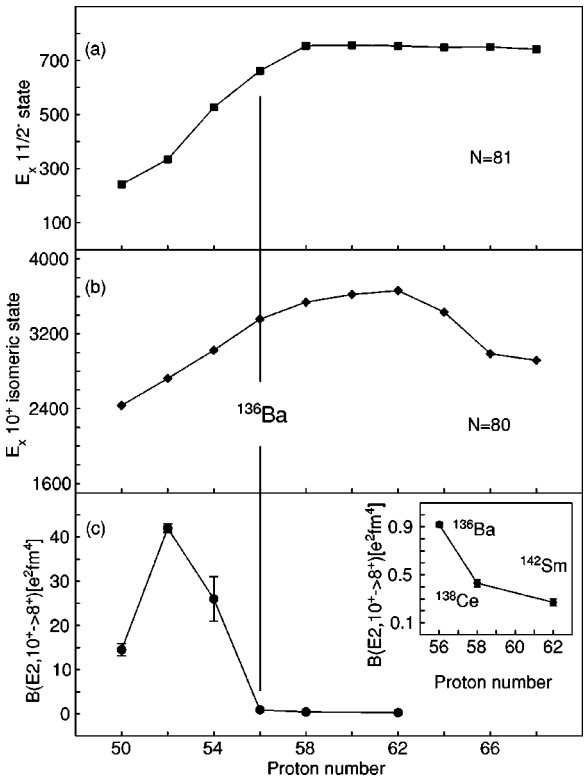

FIG. 14. Upper panel (a) shows the energies of the $I^{\pi}=\frac{11}{2}^{-}$ single-hole states for the $N=81$ isotones, taken from Ref. [23]. Panels (b) and (c) show the excitation energy of the $I^{\pi}=10^{+}$ isomer and the $B(E2:10^{+}\rightarrow 8^{+})$ transitions rates for the $N=80$ isotones, respectively, taken from Refs. [3,4,6].

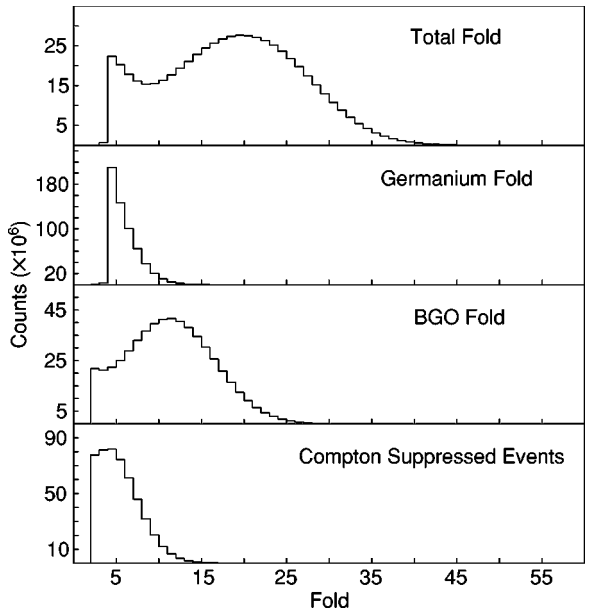

FIG. 15. Total fold measured in the reaction (top), lower panels show the different contributions. Note that the total fold (F_{tot}) shown in the upper panel is not the direct sum of the three lower panels but the addition of the three contributions ($F_{BGO}, F_{HPGe}, F_{CS}$) event by event (see text).

Compton suppressed, which were detected in all the germanium detectors, and F_{CS} are the γ rays that have been Compton suppressed, i.e., γ rays that Compton scattered out of the germanium and were detected in the HPGe detector in coincidence with its BGO shielding.

Average fold versus recoil scattering angle

Using semiclassical expressions, given in Ref. [47], an incident beam of ^{136}Xe at 850 MeV gives an initial angular momentum $L_{max}\approx 300\hbar$. From the semiclassical sticking and rolling approximations [45,48,49] one can obtain an estimate of the angular momentum input to the fragments in a given binary reaction. In the sticking limit [45] the predicted angular momentum input to the fragments for the current work is $J_{BLF}\approx 30\hbar$ and $J_{TLF}\approx 60\hbar$, while for the rolling mode limit, $J_{BLF}\approx 17\hbar$ and $J_{TLF}\approx 45\hbar$. These numbers give an indication of the spin states that might be expected to be populated in this reaction and can be compared with the average folds measured in the current work. To first order this should be related to the average number of γ rays emitted by the sum of the binary partners in a given event.

A $\gamma_{delayed}$-θ_{scatt}-*fold* cube (see Table I) was used to obtain the angular distribution of the average fold in the laboratory frame. Figure 16 shows such distributions gated on delayed γ rays in ^{136}Xe, ^{136}Ba, ^{138}Ba, and ^{125}Sb. Figure 16 has some general features. One of the most prominent is the dip in average fold around the grazing angle ($\approx 50°$). Note that this reduction in average fold is more prominent in the case of the beam ^{136}Xe than for ^{136}Ba or ^{138}Ba and it is essentially nonexistent in the case of the ^{125}Sb. A second feature is the roughly constant average fold over the angular range ($\theta=65°-85°$), where the average fold is the highest. At more forward angles ($\theta=21°-39°$) the statistics are lower, but the average fold is roughly constant in the case of ^{136}Ba, ^{138}Ba, and ^{125}Sb, unlike in ^{136}Xe where the fold at forward angle decreases due to the influence of the lower multiplicity Coulomb scattering channel. The reason why the statistics are lower at smaller angles is related to the low energy of the recoils scattered at those angles, lowering the efficiency of Chico in this angular range.

The γ-ray fold for an event gives a measure of the degree of inelasticity of the binary interaction. The greater the overlap and degree of transfer between the two fragments, the more angular momentum is transferred into the internal spins of the fragments [45]. The transfer of angular momentum in heavy-ion collisions such as those described in this paper can be studied in terms of the average fold versus the measured scattering angle of the recoils.

At the grazing angle the target and beam nuclei are expected to have a highly peripheral contact and thus quasielastic events would be expected to dominate. Since such quasielastic reactions are expected to have a relatively small transfer of angular momentum from the initial angular momentum into internal spins [50] the average multiplicity is expected to decrease in the vicinity of the grazing angle. This regime could be explained with the rolling mode. The transfer of angular momentum increases continuously with the degree of inelasticity [48], when the nuclei touch each other more solidly; if the contact time is long enough (i.e., deep-inelastic collisions), the sticking limit ought to be reached.

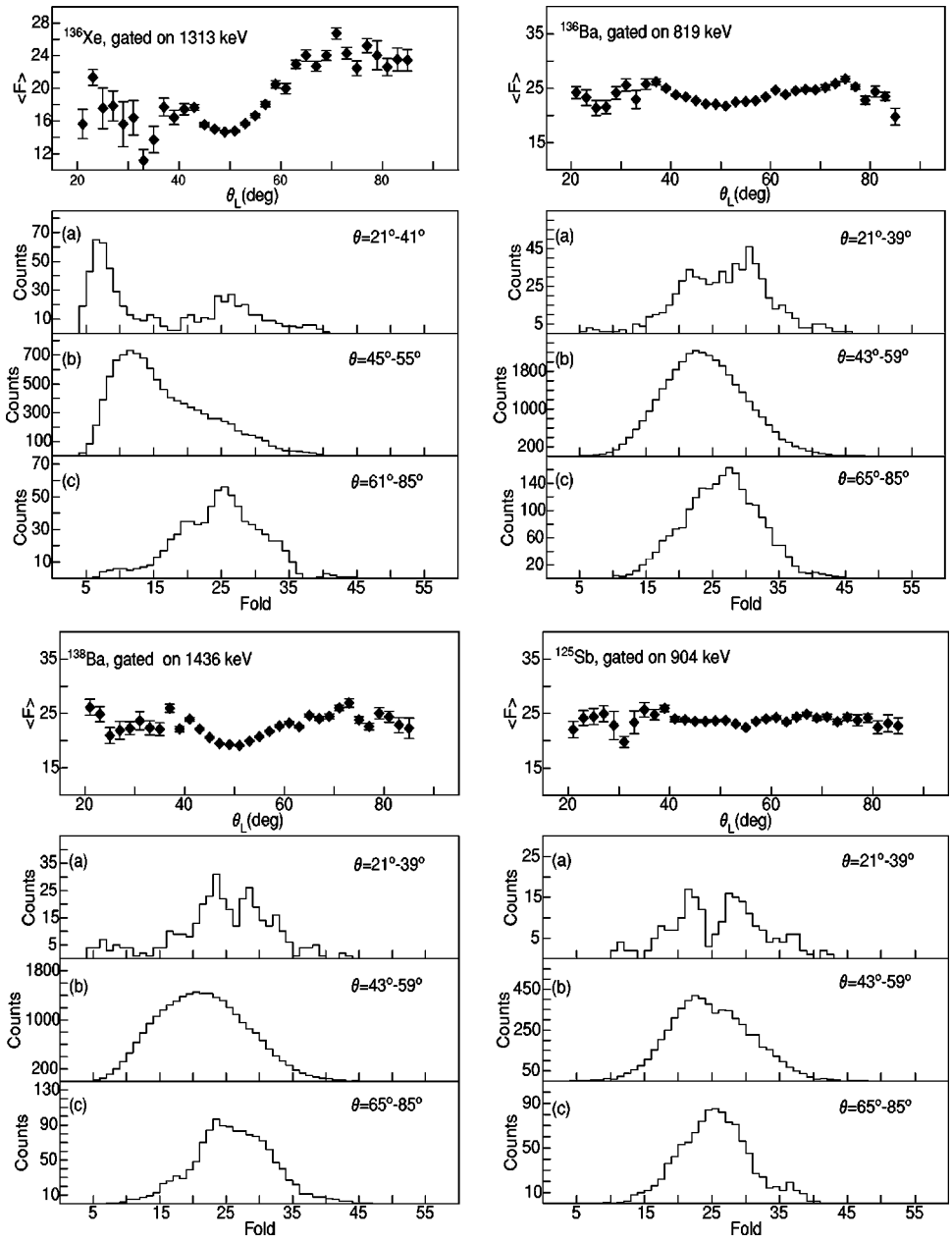

FIG. 16. Average fold distribution vs laboratory scattering recoil angle θ for the beam ^{136}Xe (top left), ^{136}Ba (top right), ^{136}Ba (bottom left), and ^{125}Sb (bottom right). In the spectra (a), (b), and (c) fold cuts for various angular ranges are shown. Note that the grazing angle in the spectrum is around 50° (see text for details).

The typical deduced γ-ray fold values of the order of 25 correspond to the *average* fold per event, however, it is worth noting that the fold distribution extends up to considerably higher values of 35 and greater, see Fig. 16. While some of this apparent increase simply reflects the response function of the GAMMASPHERE array, it is clear that significantly higher folds are populated in this mechanism, which bodes well for future high-spin studies using heavy-ion binary collisions.

VII. SUMMARY AND CONCLUSIONS

In summary, evidence for an $I^{\pi}=(10^{+})$ isomer has been reported for the first time in ^{136}Ba at an excitation energy of 3357 keV. It was produced in a binary reaction between a ^{136}Xe beam at 850 MeV impinging on a thin ^{198}Pt target. The assigned configuration is the two-neutron-hole $(\nu h_{11/2})^{-2}_{10^{+}}$ arrangement, in good agreement with the shell-model and pair-truncated shell-model predictions and the systematics of the $N=80$ isotones. The increase in excitation energy of the 10^{+} isomers and the decrease in the $B(E2)$ values along the $N=80$ isotones can be understood qualitatively in terms of the single-particle excitation energy of the $h_{11/2}$ neutron orbital. The identification of this (10^{+}) isomeric state completes the systematics for the $N=80$ isotones from the $Z=50$ closed-shell $^{130}_{50}$Sn to past the proton midshell at $^{148}_{68}$Er. Prompt decaying states above the isomer have also been identified. The half-lives of a number of isomers populated in the reaction have been reported for the first time in ^{131}I, ^{133}I, ^{184}W, ^{191}Os, ^{192}Os, and ^{198}Pt.

The momentum transfer in this reaction has been investigated in terms of the average fold versus the scattering angle of the recoils. It is crucial to study the average fold distribu-

tion of neutron-rich nuclei that can be produced via deep-inelastic processes, since spectrometers such as PRISMA [51] can use this angular information to measure recoils with the highest spin input.

ACKNOWLEDGMENTS

The authors are thankful to the staff of LBNL for providing a high-quality beam and technical support. This work was supported by EPSRC (UK) and the U.S. Department of Energy, under Grant Nos. DE-FG02-91ER-40609 and DE-AC03-76SF00098 and the National Science Foundation. A.D.Y., S.D.L., and J.J.V.D. acknowledge financial support from EPSRC. P.H.R. acknowledges support from Yale University via both the Flint and the Science Development Funds. Z.P. acknowledges financial support from EPSRC.

[1] B. Fogelberg, M. Hellström, D. Jerrestam, H. Mach, J. Blomqvist, A. Kerek, L. O. Norlin, and J. P. Omtvedt, Phys. Rev. Lett. **73**, 2413 (1994).
[2] B. Fogelberg, K. Heyde, and J. Sau, Nucl. Phys. **A352**, 157 (1981).
[3] J. Genevey, J. A. Pinston, C. Foin, M. Rejmund, R. F. Casten, H. Faust, and S. Oberstedt, Phys. Rev. C **63**, 054315 (2001).
[4] G. Lo Bianco, P. Paruzzi, K. P. Schmittgen, R. Reinhardt, A. Gelberg, K. O. Zell, P. von Brentano, and N. Blasi, Nucl. Phys. **A470**, 266 (1987).
[5] J. C. Merdinger, F. A. Beck, E. Bozek, T. Byrski, C. Gehringer, Y. Schutz, and J. P. Vivien, Nucl. Phys. **A346**, 281 (1980).
[6] M. Lach, J. Styczen, R. Julin, M. Piiparinen, H. Beuscher, P. Kleinheinz, and J. Blomqvist, Z. Phys. A **319**, 235 (1984).
[7] H. A. Roth, S. E. Arnell, D. Foltescu, Ö. Skeppstedt, J. Blomqvist, G. de Angelis, D. Bazzacco, and S. Lunardi, Eur. Phys. J. A **10**, 275 (2001).
[8] S. Harissopulos, A. Gelberg, A. Dewald, M. Hass, L. Weissman, and C. Broude, Phys. Rev. C **52**, 1796 (1995).
[9] P. Raghavan, At. Data Nucl. Data Tables **42**, 189 (1989).
[10] Z. G. Gan *et al.*, Eur. Phys. J. A (in press).
[11] P. Das *et al.*, Phys. Rev. C **53**, 1009 (1996).
[12] J. H. Hamilton *et al.*, Phys. Rep. **264**, 215 (1996).
[13] J. H. Hamilton *et al.*, Prog. Part. Nucl. Phys. **38**, 273 (1997).
[14] W. Urban *et al.*, Nucl. Phys. **A613**, 104 (1997).
[15] M. Ohshima, S. Hayashibe, N. Kawamura, Y. Itoh, M. Fujioka, and T. Ishimatsu, Hyperfine Interact. **7**, 103 (1979).
[16] W. Gelletly, J. A. Moragues, M. A. Mariscotti, and W. R. Kane, Phys. Rev. **181**, 1682 (1969).
[17] P. J. Rothschild, A. M. Baxter, S. M. Burnett, M. P. Fewell, G. J. Gyapong, and R. H. Spear, Phys. Rev. C **34**, 732 (1986).
[18] E. Dragulescu, G. Semenescu, and I. Iftimia, Pramana, J. Phys. **53**, 447 (1999).
[19] M. A. Deleplanque, Lawrence Berkeley National Laboratory Report No. 5202, 1988.
[20] M. W. Simon, D. Cline, C. Y. Wu, R. W. Gray, R. Teng, and C. Long, Nucl. Instrum. Methods Phys. Res. A **452**, 205 (2000).
[21] P. E. Hodgson, *Nuclear Heavy-Ion Reactions* (Oxford University Press, Oxford, 1978).
[22] T. Glasmacher, Annu. Rev. Nucl. Part. Sci. **48**, 1 (1998).
[23] *Table of Isotopes*, 8th ed., edited by R. B. Firestone and V. S. Shirley (Wiley, New York, 1996).
[24] L. C. Carraz, J. Blachot, E. Monnand, and A. Moussa, Nucl. Phys. **A158**, 403 (1970).
[25] D. C. Radford, Nucl. Instrum. Methods Phys. Res. A **361**, 297 (1995).
[26] W. Urban (private communication).
[27] A. Kerek, P. Carlé, and J. McDonald, Nucl. Phys. **A198**, 466 (1972).
[28] A. Kerek, A. Luukko, M. Grecescu, and J. Sztarkier, Nucl. Phys. **A172**, 603 (1971).
[29] L. C. Carraz, E. Monnand, and A. Moussa, Nucl. Phys. **A171**, 209 (1971).
[30] M. Kortelahti, A. Pakkanen, M. Piiparinen, T. Komppa, and R. Komu, Nucl. Phys. **A376**, 1 (1982).
[31] C. Wheldon *et al.*, Eur. Phys. J. A (in press).
[32] M. Pfützner *et al.*, Phys. Rev. C **65**, 064604 (2002).
[33] Zs. Podolyák, M. Caamaño, P. H. Regan, P. M. Walker, P. Mayet, J. Gerl, Ch. Schlegel, M. Hellström, M. Mineva, and M. Pfützner, Prog. Theor. Phys. **146**, 467 (2002).
[34] J. C. Cunnane, M. Piiparinen, and P. J. Daly, Phys. Rev. C **13**, 2197 (1976).
[35] V. Kölschbach, P. Schüler, K. Hardt, D. Rosendaal, C. Günther, K. Euler, R. Tölle, M. Marten-Tölle, and P. Zeyen, Nucl. Phys. **A439**, 189 (1985).
[36] C. T. Zhang *et al.*, Nucl. Phys. **A628**, 386 (1998).
[37] M. Meyer-Lévy and V. Lopac, Phys. Rev. C **8**, 829 (1973).
[38] K. Higashiyama, N. Yoshinaga, and K. Tanabe, Phys. Rev. C **65**, 054317 (2002).
[39] K. Higashiyama, N. Yoshinaga, and K. Tanabe, Phys. Rev. C **67**, 044305 (2003).
[40] A. Bohr and B. Mottelson, *Nuclear Structure* (Benjamin, New York, 1975), Vol. 1.
[41] T. R. Fisher and P. D. Bond, Part. Nuclei **6**, 119 (1973).
[42] C. Bargholtz, L. Eriksson, L. Gidefeldt, L. Holmberg, and V. Stefansson, Z. Phys. **260**, 1 (1973).
[43] S. Z. Gui, G. Colombo, and E. Nolte, Z. Phys. A **305**, 297 (1982).
[44] E. Nolte, G. Colombo, S. Z. Gui, G. Korschinek, W. Schollmeier, P. Kubik, S. Gustavsson, R. Geier, and H. Morinaga, Z. Phys. A **306**, 211 (1982).
[45] R. Bock *et al.*, Nukleonika **22**, 529 (1977).
[46] S. J. Asztalos *et al.*, Phys. Rev. C **60**, 044307 (1999).
[47] D. A. Bromley, *Treatise on Heavy-Ion Science* (Plenum, New York, 1984), Vol. 4.
[48] M. Lefort and Ch. Ngô, Ann. Phys. **3**, 5 (1978).
[49] H. Takai *et al.*, Phys. Rev. C **38**, 1247 (1988).
[50] A. Olmi *et al.*, Phys. Rev. Lett. **41**, 688 (1978).
[51] A. M. Stefanini *et al.*, Nucl. Phys. **A701**, 217c (2001).